International Journal of Science and Engineering Applications
Volume 4 Issue 2, 2015, ISSN-2319-7560 (Online)

Effect of Titanium Oxide on Structure, Bearing Properties of Tin-Antimony-Lead and Tin-Aluminum Alloys

Abu Bakr El- Bediwi
Metal Physics Lab., Physics Department, Faculty of Science, Mansoura University
Mansoura, Egypt

Abbas Al- Bawee
Faculty of engineering, University of Diayala
Diayala, Iraq

Mustafa Kamal
Metal Physics Lab., Physics Department, Faculty of Science, Mansoura University
Mansoura, Egypt

Abstract: Effect of adding titanium oxide nanoparticles (TiO_2) on structure, elastic moduli, Vickers hardness, internal friction, electrical resistivity and thermal properties of tin-antimony-lead and tin-aluminum bearing alloys have been investigated. Elastic modulus, Vickers hardness and thermal diffusivity of $Sn_{87}Sb_{10}Pb_3$ and $Sn_{80}Al_{20}$ alloys increased after adding TiO_2 nanoparticles. Internal friction, thermal conductivity and specific heat of $Sn_{87}Sb_{10}Pb_3$ and $Sn_{80}Al_{20}$ alloys varied after adding TiO_2 nanoparticles. Adding titanium oxide nanoparticles improved bearing properties, such as strengthens and internal friction of $Sn_{87}Sb_{10}Pb_3$ and $Sn_{80}Al_{20}$ alloys. The $Sn_{85.5}Sb_{10}Pb_3(TiO_2)_{1.5}$ alloy has best properties for automotive industry. Also $Sn_{78.5}Al_{20}(TiO_2)_{1.5}$ alloy has best properties for marine applications.

Key words: titanium oxide, internal friction, thermal properties, structure, hardness, resistivity, bearing alloys

Introduction

Bearings are used to prevent friction between parts during relative movement. In machinery they fall into two primary categories: anti-friction or rolling element bearings and hydrodynamic journal bearings. Today, the term Babbitt covers a collection of “white metal” alloys consisting generally of a tin or lead base accompanied by antimony and copper. Babbitt metal is used as the lining for bearing shells of cast iron, steel and bronze. Fry manufactures two basic types of babbitt, high-tin alloys and high-lead alloys. Both are relatively low melting materials consisting of hard compound in a soft matrix. Al–Sn alloys have a very long history (Forrester 1960) to be used as bearing materials [1]. These alloys provide a good combination of strength and surface properties [2]. The fatigue strength of cold worked and heat treated Al–20%Sn–1%Cu alloy having reticular structure is close to that of Cu–30%Pb alloy with higher seizure resistance [3]. Aluminium has a low modulus of elasticity and apart from indium, lead has the lowest modulus of elasticity of all the soft phases alloying with aluminium [4]. Al-Sn based alloys are widely used as sliding bearing materials in automobile and shipbuilding industry [5, 6]. HVOF spray process has been introduced by McCartney to prepare Al-Sn-Si bearing alloy coatings. Post heat treatment of the HVOF sprayed coating at 300 ºC proved the coarsening of tin and precipitate of Si in the coating [7, 8]. Based on the feasibility of preparing oxygen sensitive metal coatings, cold spray was also introduced to deposit Al-Sn binary alloy coatings [9]. Al-5Sn coating can be deposited by high pressure cold spray with nitrogen while Al-10Sn can only be deposited by low pressure cold spray with helium gas. Both Al-5Sn and Al-10Sn coatings present dense structures. The coarsening and/or migration of Sn phase in the coatings were observed when the annealing temperature exceeds 200 ºC. Furthermore, the microhardness of the coatings decreased significantly at the annealing temperature of 250 ºC [10]. Aluminum tin and leaded aluminium alloys slightly differ in mechanical properties. Frictional states created during sliding against steel shaft under oil lubrication were not much different. Leaded aluminium alloy bushes show marginally lower friction than the conventional ones [11]. Adding Cu/Pb to Sn-Sb alloy improve their elastic modulus, internal friction, hardness and thermal conductivity [12]. The friction coefficients of Sn-20.2%Sb-16.6%Pb-2.6%Cu are lower than that of Sn–7.2%Sb–0.4%Pb–3%Cu under all scratch test conditions [13]. Structure, hardness, mechanical and electrical transport properties of $Sn_{90-x}Sb_{10}Bi_x$ ($x = 0$, or $x \geq 1$) alloys have been studied and analyzed [14]. The effects of solidification rate and microadditions on mechanical properties and micromorphology of $SnSb_{10.4}$ alloy have been studied [15]. Creep behaviour, elastic modulus and internal friction of $SnSb_{10}Cu_2X_2$ (X=Pb, Ag, Se, Cd and Zn) alloys have been investigated also stress exponent values have been determined using Mulhearn-Tabor method [16]. The aim of this research was to investigate the effect of adding titanium oxide nanoparticles (TiO_2) on structure, elastic moduli, Vickers hardness, internal friction and thermal properties of tin-antimony-lead and tin-aluminum bearing alloys.

Experimental work

Two groups of quaternary bearing alloys, tin- antimony-lead- titanium oxide and tin- aluminum- titanium oxide, were used. These groups' alloys were molten in the muffle furnace using (high purity more than 99.95%) tin, antimony, lead, aluminum and titanium oxide. The resulting ingots were turned and re-melted several times to increase the homogeneity of the ingots. From these ingots, long ribbons of about 3-5 mm width and ~ 70 µm thickness were prepared as the test samples by directing a stream of molten alloy onto the outer surface of rapidly revolving copper roller with surface velocity 31 m/s giving a cooling rate of 3.7×10^5 k/s. The samples then cut into convenient shape for the measurements using double knife cuter. Structure of used alloys was performed using an Shimadzu X–ray Diffractometer (Dx–30, Japan)of Cu–Kα radiation with λ=1.54056 Å at 45 kV and 35 mA and Ni–filter in the angular range 2θ ranging from 0 to 100° in continuous mode with a scan speed 5 deg/min. Electrical resistivity of used alloys was measured by double bridge method. The melting endotherms of used alloys were obtained using a SDT Q600 V20.9 Build 20 instrument. A digital Vickers micro-hardness tester, (Model-FM-7- Japan), was used to measure Vickers hardness values of used alloys. Q^{-1}, the elastic modulus E and thermal diffusivity D_{th} of used alloys were determined using the dynamic resonance method [17- 19].

$$\left(\frac{E}{\rho}\right)^{1/2} = \frac{2\pi L^2 f_o}{kz^2}$$

$$Q^{-1} = 0.5773\frac{\Delta f}{f_o}$$

$$D_{th} = \frac{2d^2 f_o}{\pi}$$

Where ρ is the density of the sample under test, L is the length of the vibrated part of the sample, k is the radius of gyration of cross section perpendicular to its plane of motion, f_0 is the resonance frequency and z is the constant depends on the mode of vibration and is equal to 1.8751. Δf is the half width of the resonance curve.

Results and discussions

Effect of adding TiO_2 nanoparticles on structure of Sn-Sb-Pb alloy

X-ray diffraction patterns of $Sn_{87-x}Sb_{10}Pb_3(TiO_2)_x$ (x=0.5, 1 and 1.5 wt. %) rapidly solidified alloys have lines corresponding to β- Sn, Pb/or Sb and SbSn intermetallic phases as shown in Figure 1. X-ray analysis show that, adding TiO_2 to $Sn_{87}Sb_{10}Pb_3$ alloy caused a change in Sn matrix structure such as lattice parameters and formed crystal structure (crystallinity, crystal size and the orientation) as seen in Table 1(a and b). That is because TiO_2 nanoparticles dissolved in Sn matrix formed a solid solution and other accumulated particles formed a traces of phases.

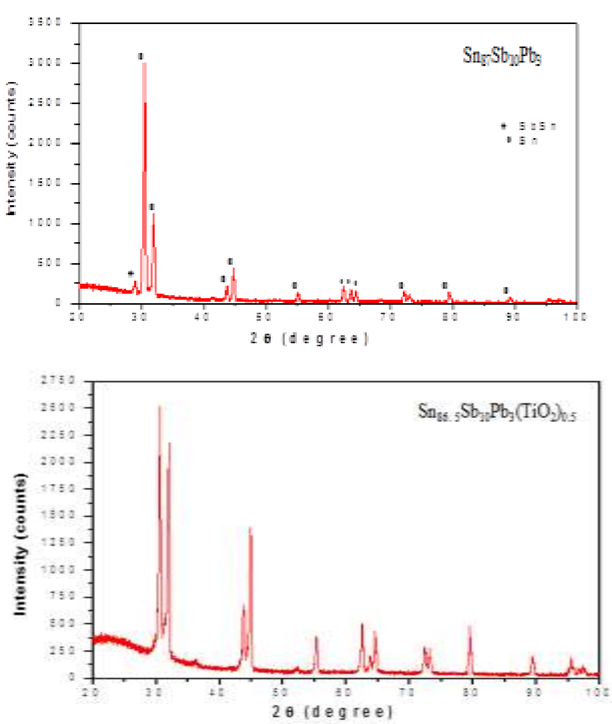

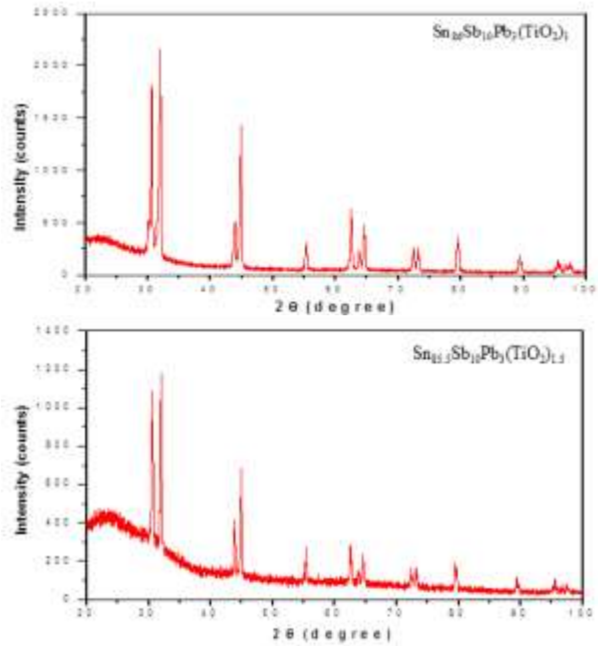

Figure 1:- x-ray diffraction patterns of $Sn_{87-x}Sb_{10}Pb_3(TiO_2)_x$ alloys

Table 1a:- x-ray diffraction analysis of $Sn_{87-x}Sb_{10}Pb_3(TiO_2)_x$ alloys

$Sn_{87}Sb_{10}Pb_3$					
2θ	d Å	Int.%	FWHM	Phase	hkl
29.0695	3.07186	4.37	0.2755	SbSn	101
30.4985	2.92868	100	0.2400	Sn	200
30.6095	2.92557	69.41	0.0720	Sn	200
31.9779	2.796439	34.11	0.1920	Sn	101
41.5347	2.17246	0.77	0.5760	SbSn	012
43.6580	2.07160	5.13	0.4320	Sn	220
44.7618	2.02304	12.29	0.3360	Sn	211
55.1013	1.66539	3.75	0.3360	Sn	301
62.4237	1.48648	5.81	0.3360	Sn	112
63.6354	1.46106	4.05	0.3840	Sn	400
64.3731	1.44609	3.59	0.4320	Sn	321
68.2871	1.37243	0.41	0.5760	SbSn	113
72.1128	1.30874	3.63	0.2880	Sn	420
72.9123	1.29635	2.75	0.2880	Sn	411
79.3161	1.20698	3.59	0.2880	Sn	321
89.0610	1.09840	2.05	0.2400	Sn	432
95.3295	1.04205	1.46	0.3840	Sn	103
96.3177	1.03396	0.64	0.4800	Sn	330
97.0846	1.02783	0.75	0.4800	Sn	521

$Sn_{86.5}Sb_{10}Pb_3(TiO_2)_{0.5}$					
2θ	d Å	Int.%	FWHM	Phase	hkl
30.6118	2.92052	100	0.2558	Sn	200
32.0305	2.79433	80.39	0.2558	Sn	101
36.1764	2.48304	1.74	0.4723	Pb	220
43.7948	2.06715	25.53	0.3346	Sn	220
44.8366	2.02152	56.58	0.2952	Sn	211
52.2999	1.74926	1.68	0.3936	SbSn	021
55.2681	1.66214	13.94	0.2755	Sn	301
62.4854	1.48639	18.62	0.2558	Sn	112
63.759	1.45974	5.28	0.2755	Sb	107
64.5448	1.44385	16.61	0.2165	Sn	321
72.3498	1.30611	10.53	0.2165	Sb	018
73.1307	1.29409	8.95	0.2558	Sn	411
79.4279	1.20656	16.98	0.1968	Sn	321
89.2927	1.09706	6.94	0.1968	Sn	432
95.4951	1.04154	6.04	0.1968	Sn	103
96.6061	1.0325	1.82	0.2362	Sn	440
97.2882	1.02622	3.09	0.24	Sn	521

$Sn_{86}Sb_{10}Pb_3(TiO_2)_1$					
2θ	d Å	Int.%	FWHM	Phase	hkl
30.6133	2.92038	86.52	0.2558	Sn	200
32.0016	2.79679	100	0.2558	Sn	101
43.8373	2.06525	22.17	0.2755	Sn	220
44.8304	2.02178	66.02	0.2362	Sn	211
55.2842	1.66169	12.86	0.3346	Sn	301
62.4583	1.48697	25.71	0.2558	Sn	112
63.7276	1.46038	7.61	0.2165	Sb	107
64.4749	1.44525	17.75	0.2165	Sn	321
72.3608	1.30594	10.42	0.1771	Sb	018
73.0899	1.29471	10.52	0.1771	Sn	411
79.4307	1.20552	15.71	0.264	Sn	321
79.7468	1.20453	8.87	0.192	Sn	321
89.3151	1.09594	7.47	0.264	Sn	432
89.6708	1.09523	4.46	0.192	Sn	431
95.0358	1.04449	1.75	0.24	Sn	103
95.5155	1.04051	5.28	0.216	Sn	103
95.8764	1.04013	3.21	0.216	Sn	332
96.6134	1.03158	3.09	0.24	Sn	440
97.3745	1.02554	4.55	0.24	Sn	521

$Sn_{85.5}Sb_{10}Pb_3(TiO_2)_{1.5}$					
2θ	d Å	Int.%	FWHM	Phase	hkl
30.6023	2.9214	88.93	0.2755	Sn	200
32.0244	2.79485	100	0.2558	Sn	101
43.8265	2.06574	31.18	0.1968	Sn	220
44.9301	2.01753	60.27	0.2362	Sn	211
55.2598	1.66237	16.36	0.1771	Sn	301
62.4719	1.48668	20.78	0.1968	Sn	112
63.8004	1.45889	5.73	0.3149	Sb	107
64.5084	1.44458	14.03	0.1968	Sn	321
72.3331	1.30638	8.85	0.1574	Sb	018
73.1077	1.29444	10.06	0.1771	Sn	411
79.417	1.2067	12.82	0.1771	Sn	321
89.3181	1.09682	7.16	0.1771	Sn	432
95.4954	1.04154	7.27	0.1771	Sn	103
97.4966	1.02458	2.88	0.576	Sn	521

Table 1b:- lattice parameters and crystal size of β-Sn in $Sn_{87-x}Sb_{10}Pb_3(TiO_2)_x$ alloys

Alloys	a Å	c Å	V $Å^3$	τ Å
$Sn_{87}Sb_{10}Pb_3$	5.857	3.174	108.883	355.44
$Sn_{86.5}Sb_{10}Pb_3(TiO_2)_{0.5}$	5.841	3.18	108.62	514.283
$Sn_{86}Sb_{10}Pb_3(TiO_2)_1$	5.841	3.2	109.15	508.035
$Sn_{85.5}Sb_{10}Pb_3(TiO_2)_{1.5}$	5.843	3.19	108.83	529.678

Scanning electron micrographs, SEM, of $Sn_{87-x}Sb_{10}Pb_3(TiO_2)_x$ (x=0 and 1.5 wt. %) alloys show heterogeneity structure as shown in Figure 2. SEM micrographs of $Sn_{87-x}Sb_{10}Pb_3(TiO_2)_x$ alloys show β- Sn matrix and other accumulated particles formed traces of phases and that is agreed with x-ray results.

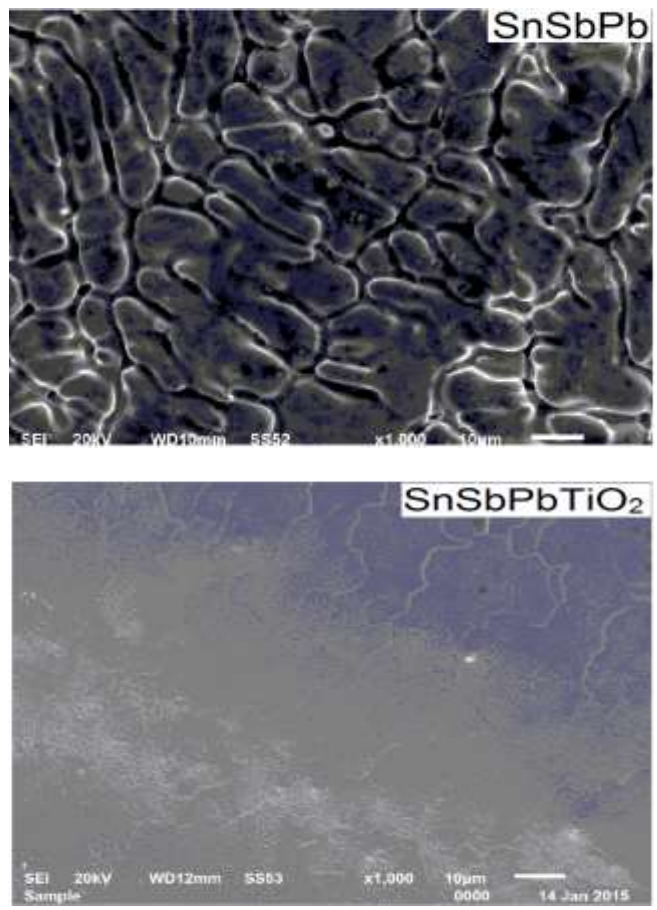

Figure 2:- SEM of $Sn_{87}Sb_{10}Pb_3$ and $Sn_{85.5}Sb_{10}Pb_3(TiO_2)_{1.5}$ alloys

Effect of adding TiO_2 nanoparticles on mechanical properties of Sn-Sb-Pb alloy

The elastic constants are directly related to atomic bonding and structure. Elastic modului of $Sn_{87-x}Sb_{10}Pb_3(TiO_2)_x$ alloys are listed in Table 2. Elastic modulus of $Sn_{87}Sb_{10}Pb_3$ alloy increased after adding different ratio from TiO_2 nanoparticles. The $Sn_{85.5}Sb_{10}Pb_3(TiO_2)_{1.5}$ alloy has highest elastic modulus.

Table 2:- elastic modului, internal friction and thermal diffusivity of $Sn_{87-x}Sb_{10}Pb_3(TiO_2)_x$ alloys

Alloys	E GPa	μ GPa	B GPa	Q^{-1}	D_{th} x10^{-8} m^2\sec
$Sn_{87}Sb_{10}Pb_3$	33.02	12.15	39.15	0.025	9.43
$Sn_{86.5}Sb_{10}Pb_3(TiO_2)_{0.5}$	38.3	14.1	45.3	0.031	27.36
$Sn_{86}Sb_{10}Pb_3(TiO_2)_1$	39.1	14.4	46.1	0.024	21.43
$Sn_{85.5}Sb_{10}Pb_3(TiO_2)_{1.5}$	47.2	17.4	55.4	0.018	41.87

The resonance curves $Sn_{87-x}Sb_{10}Pb_3(TiO_2)_x$ alloys are shown in Figure 3. Calculated internal friction and thermal diffusivity of $Sn_{87-x}Sb_{10}Pb_3(TiO_2)_x$ alloys are listed in Table 2. Internal friction of $Sn_{87}Sb_{10}Pb_3$ alloy varied after adding different ratio from TiO_2 nanoparticles. The $Sn_{85.5}Sb_{10}Pb_3(TiO_2)_{1.5}$ alloy has lowest internal friction.

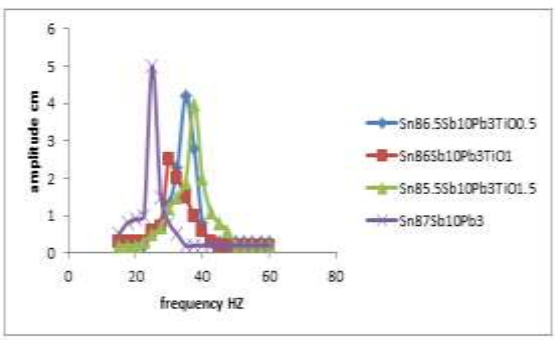

Figure 3:- resonance curves of $Sn_{87-x}Sb_{10}Pb_3(TiO_2)_x$ alloys

The hardness is the property of material, which gives it the ability to resist being permanently deformed when a load is applied. Vickers hardness of $Sn_{87-x}Sb_{10}Pb_3(TiO_2)_x$ alloys at 10 gram force and indentation time 5 sec are shown in Table 3. The minimum shear stress (τ_m) value of $Sn_{87-x}Sb_{10}Pb_3(TiO_2)_x$ alloys was calculated using the equation [9], where ν is Poisson's ratio of the elements in the alloy and then listed in Table 3.

$$\tau_m = \frac{1}{2}\, H_v \left\{ \frac{1}{2}(1-2\nu) + \frac{2}{9}(1+\nu)[2(1+\nu)]^{\frac{1}{2}} \right\}$$

Vickers hardness of $Sn_{87}Sb_{10}Pb_3$ alloy increased after adding TiO_2 nanoparticles. That is because TiO_2 dissolved in Sn matrix formed a hard inclusion increased its hardness. $Sn_{85.5}Sb_{10}Pb_3(TiO_2)_{1.5}$ alloy has highest hardness.

Table 3:- Vickers hardness and minimum shear stress of $Sn_{87-x}Sb_{10}Pb_3(TiO_2)_x$ alloys

Alloys	H_v kg/mm^2	μ_s kg/mm^2
$Sn_{87}Sb_{10}Pb_3$	28.52±1.8	9.41
$Sn_{86.5}Sb_{10}Pb_3(TiO_2)_{0.5}$	31.68±2.7	10.45
$Sn_{86}Sb_{10}Pb_3(TiO_2)_1$	36.53±3.3	12.05
$Sn_{85.5}Sb_{10}Pb_3(TiO_2)_{1.5}$	38.83±2.4	12.81

Effect of adding TiO_2 on thermal properties and electrical resistivity of Sn- Sb- Pb alloy

Thermal analysis is often used to study solid state transformations as well as solid-liquid reactions. Figure 4 shows DSC thermographs for $Sn_{87-x}Sb_{10}Pb_3(TiO_2)_x$ alloys. Little variation occurred in exothermal peak of $Sn_{87}Sb_{10}Pb_3$ alloy. The melting temperature and other thermal properties of $Sn_{87-x}Sb_{10}Pb_3(TiO_2)_x$ alloys are listed in Table 4. Melting temperature of $Sn_{87}Sb_{10}Pb_3$ alloy decreased after adding TiO_2 nanoparticles.

Crystalline defects serve as scattering center for conduction electrons in metals, so the increase in their number raises the imperfection. Electrical resistivity and calculated thermal conductivities of $Sn_{87-x}Sb_{10}Pb_3(TiO_2)_x$ alloys are shown in Table 4. Electrical resistivity of $Sn_{87}Sb_{10}Pb_3$ alloy varied after adding TiO_2 nanoparticles. That is because TiO_2 nanoparticles dissolved in the Sn matrix playing as scattering center for conduction electrons caused a change in matrix structure.

Table 4:- electric resistivity and other thermal properties of $Sn_{87-x}Sb_{10}Pb_3(TiO_2)_x$ alloys

Alloys	ρ x10^{-6} Ω.cm	K W $m^{-1}K^{-1}$	C_p x 10^3 J/kg. k	Melting point ºC
$Sn_{87}Sb_{10}Pb_3$	67.3	2.30	1.84	236.87
$Sn_{86.5}Sb_{10}Pb_3(TiO_2)_{0.5}$	59.04	2.55	1.88	223.38
$Sn_{86}Sb_{10}Pb_3(TiO_2)_1$	65.19	2.32	3.93	229.52
$Sn_{85.5}Sb_{10}Pb_3(TiO_2)_{1.5}$	77.78	1.94	3.29	229.33

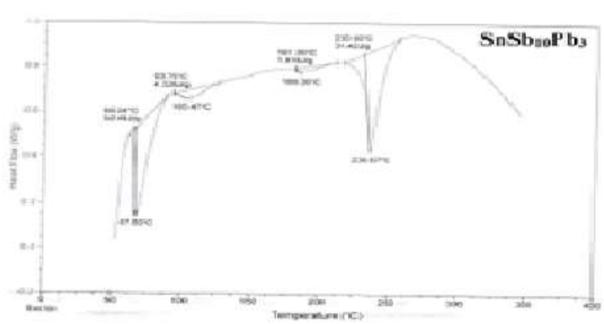

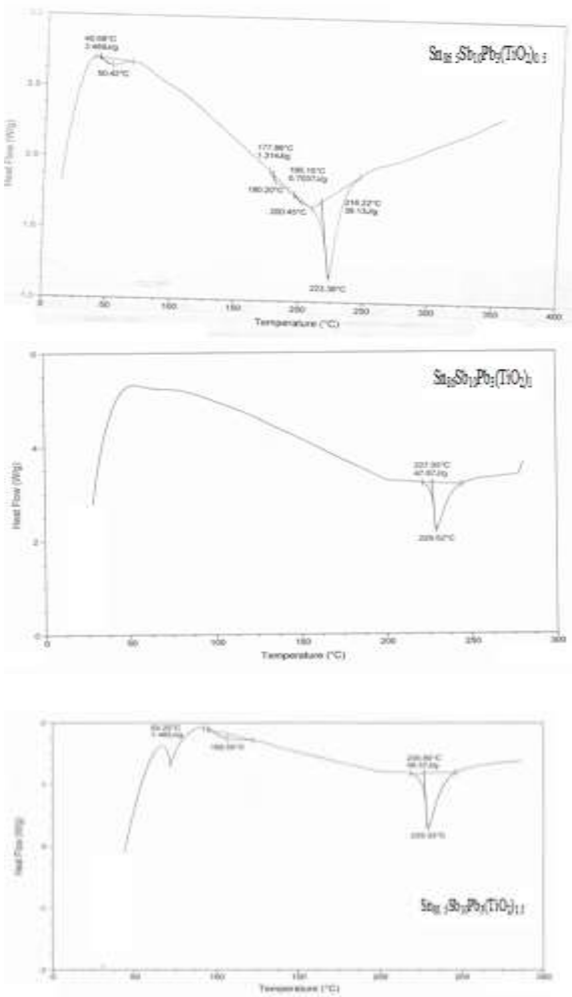

Figure 4:- DSC of $Sn_{87-x}Sb_{10}Pb_3(TiO_2)_x$ alloys

Effect of adding TiO_2 nanoparticles on structure of Sn-Al alloy

X-ray diffraction patterns of $Sn_{80-x}Al_{20}(TiO_2)_x$ (x=0.5, 1 and 1.5 wt. %) alloys have lines corresponding to β- Sn and Al phases as shown in Figure 5. X-ray analysis show that, adding TiO_2 to $Sn_{80}Al_{20}$ alloy caused a change in Sn matrix such as lattice parameters and formed crystal structure (crystallinity, crystal size and the orientation) as seen in Table 5 (a and b). That is because TiO_2 nanoparticles dissolved in Sn matrix formed a solid solution and other accumulated particles formed a traces of phases.

Scanning electron micrographs, SEM, of $Sn_{80-x}Al_{20}(TiO_2)_x$ alloys show heterogeneity structure as shown in Figure 6. SEM micrographs of $Sn_{80-x}Al_{20}(TiO_2)_x$ alloys show β- Sn matrix with other accumulated particles formed traces of phases and that agree with x-ray results

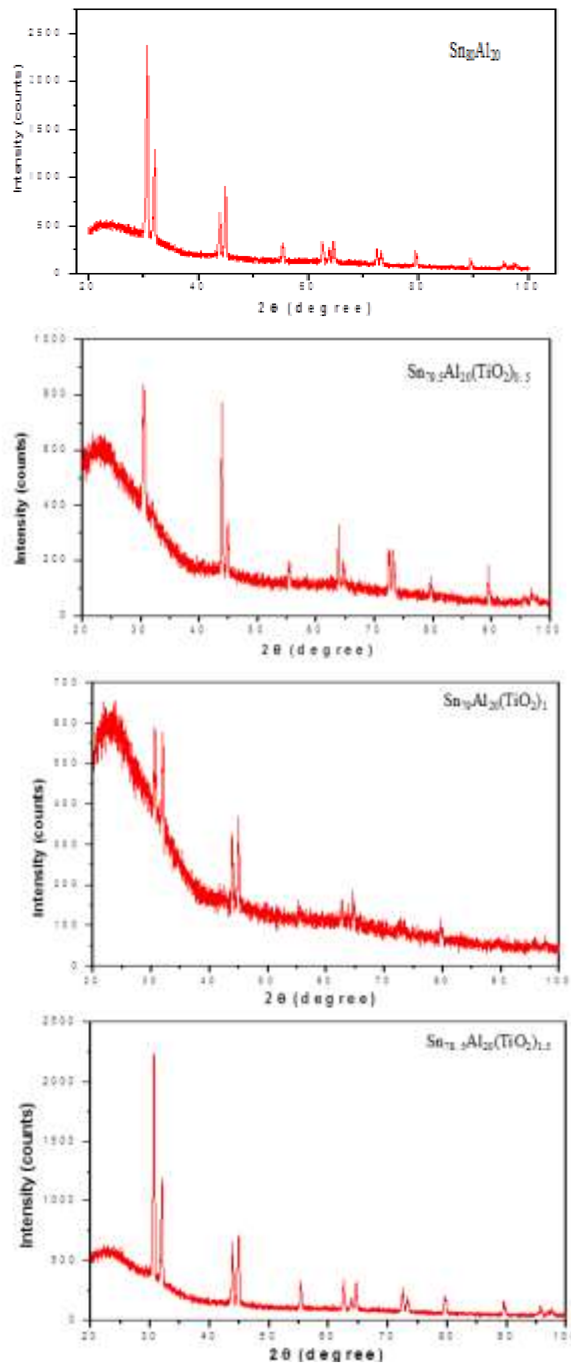

Figure 5:- x-ray diffraction patterns of $Sn_{80-x}Al_{20}(TiO_2)_x$ alloys

73.45	1.28925	6.09	0.09	Sn	411
79.7057	1.20206	11.97	0.576	Sn	321
89.61	1.094	4.68	0.09	Sn	432
95.67	1.0401	3.28	0.09	Sn	103
97.69	1.02391	7.02	0.09	Sn	521

Table 5a:- x-ray diffraction analysis of $Sn_{80-x}Al_{20}(TiO_2)_x$ alloys

$Sn_{80}Al_{20}$					
2θ	d Å	Int.%	FWHM	Phase	hkl
30.5888	2.92025	100	0.12	Sn	200
30.6656	2.92035	84.96	0.096	Sn	200
31.9935	2.79516	46.62	0.216	Sn	101
43.7803	2.0661	22.91	0.168	Sn	220
44.8271	2.02025	33.94	0.12	Al	200
55.2821	1.66037	9.25	0.432	Sn	301
62.448	1.48596	9.2	0.24	Sn	112
63.7441	1.45883	6.57	0.288	Sn	400
64.4962	1.44363	10.04	0.24	Al/Sn	220/321
72.3591	1.30489	7.2	0.192	Sn	411
73.0968	1.29353	6.01	0.336	Sn	411
79.4138	1.20574	7.3	0.24	Sn	312
89.3336	1.09576	4.52	0.192	Sn	431
95.6292	1.03957	1.42	0.768	Sn	103
97.3885	1.02543	2.57	0.288	Sn	521

$Sn_{79.5}Al_{20}(TiO_2)_{0.5}$					
2θ	d Å	Int.%	FWHM	Phase	hkl
30.378	2.94246	63.71	0.2362	Sn	200
31.9942	2.79742	31.75	0.5987	Sn	101
43.8632	2.06409	100	0.2165	Sn	220
44.8424	2.02127	28.31	0.3542	Al	211
55.3888	1.6588	12.76	0.3542	Sn	301
62.57	1.48458	4.01	0.09	Sn	112
63.8227	1.45843	25.99	0.1771	Sn	400
64.6647	1.44146	12.5	0.3149	Al/Sn	220/321
72.4103	1.30409	22.83	0.192	Sn	420
73.158	1.29367	22.73	0.1771	Sn	411
79.5208	1.20538	9.17	0.3149	Sn	321
89.4656	1.09539	17.47	0.1771	Sn	431
95.6294	1.04043	2.83	0.4723	Sn	103
96.8422	1.02975	4.62	0.576	Sn	521

$Sn_{79}Al_{20}(TiO_2)_1$					
2θ	Åd	Int.%	FWHM	Phase	hkl
30.6095	2.92074	100	0.2755	Sn	200
31.9936	2.79747	97.65	0.2362	Sn	101
43.9771	2.05901	67.42	0.2165	Sn	220
45.0299	2.01329	74.49	0.3346	Sn	211
55.41	1.65822	11.24	0.09	Sn	301
62.6126	1.48368	22.27	0.2362	Sn	112
64.6723	1.44131	25.72	0.2362	Al/Sn	220/321
72.67	1.30115	10.3	0.09	Sn	420

$Sn_{78.5}Al_{20}(TiO_2)_{1.5}$					
2θ	Åd	Int.%	FWHM	Phase	hkl
30.6183	2.91991	100	0.2558	Sn	200
32.0071	2.79632	45.14	0.2362	Sn	101
43.9365	2.06082	23.02	0.2558	Sn	220
44.8952	2.01901	30.74	0.2952	Al	211
55.3468	1.65996	10.96	0.2558	Sn	301
62.5078	1.48591	11.37	0.2362	Sn	112
63.8614	1.45764	4.34	0.1968	Sb	107
64.6256	1.44224	10.87	0.2165	Al/Sn	220/321
72.3939	1.30543	8.51	0.1968	Sb	018
73.2067	1.29293	5.95	0.1771	Sn	411
79.4578	1.20618	6.76	0.1771	Sn	321
89.3848	1.09617	4.78	0.1968	Sn	432
95.5964	1.04071	3.69	0.1771	Sn	103
97.5817	1.02391	1.68	0.576	Sn	521

Table 5b:- lattice parameters and crystal size of β-Sn in $Sn_{80-x}Al_{20}(TiO_2)_x$ alloys

Alloys	a Å	c Å	V $Å^3$	τ Å
$Sn_{80}Al_{20}$	5.841	3.19	108.65	461.64
$Sn_{79.5}Al_{20}(TiO_2)_{0.5}$	5.88	3.10	106.42	390.49
$Sn_{79}Al_{20}(TiO_2)_1$	5.84	3.16	107.69	689.284
$Sn_{78.5}Al_{20}(TiO_2)_{1.5}$	5.84	3.17	108.08	432.55

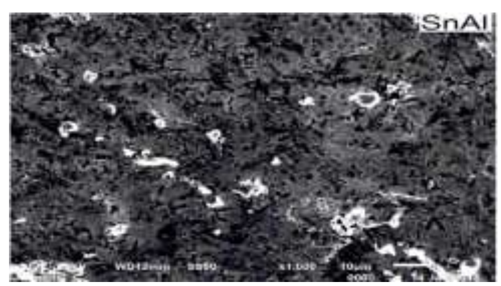

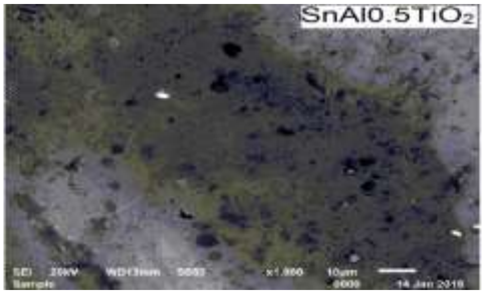

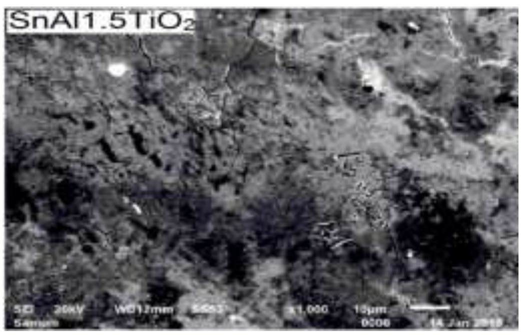

Figure 6:- SEM of $Sn_{80-x}Al_{20}(TiO_2)_x$ alloys

Effect of adding TiO_2 nanoparticles on mechanical properties of Sn- Al alloy

Elastic modului of $Sn_{80-x}Al_{20}(TiO_2)_x$ alloys are listed in Table 6. Elastic modulus of $Sn_{80}Al_{20}$ alloy increased after adding different ratio from TiO_2 nanoparticles. The $Sn_{78.5}Al_{20}(TiO_2)_{1.5}$ alloy has highest elastic modulus.

The resonance curves $Sn_{80-x}Al_{20}(TiO_2)_x$ alloys are shown in Figure 7. Calculated internal friction and thermal diffusivity of $Sn_{80-x}Al_{20}(TiO_2)_x$ alloys are listed in Table 6. Internal friction of $Sn_{80}Al_{20}$ alloy increased after adding different ratio from TiO_2 nanoparticles. The $Sn_{78.5}Al_{20}(TiO_2)_{1.5}$ alloy has high internal friction value.

Table 6:- elastic modului, internal friction and thermal diffusivity of $Sn_{80-x}Al_{20}(TiO_2)_x$ alloys

Alloys	E GPa	μ GPa	B GPa	Q^{-1}	D_{th} x10^{-8} (m^2/sec)
$Sn_{80}Al_{20}$	31.85	11.73	37.38	0.011	10.89
$Sn_{79.5}Al_{20}(TiO_2)_{0.5}$	37.6	13.9	44	0.024	24.6
$Sn_{79}Al_{20}(TiO_2)_1$	38.9	14.3	45.4	0.0227	60.97
$Sn_{78.5}Al_{20}(TiO_2)_{.1.5}$	40.8	15	47.4	0.0228	9.60

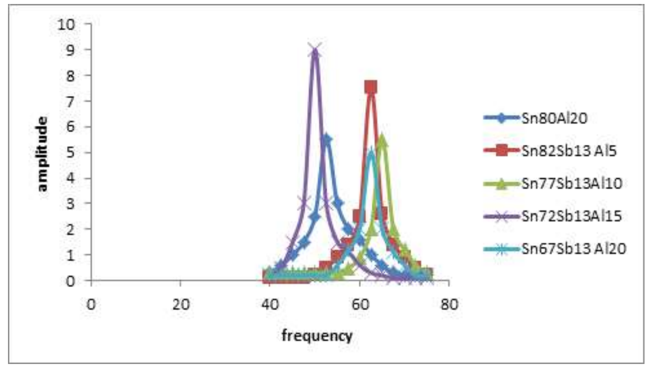

Figure 7:- resonance curves of $Sn_{80-x}Al_{20}(TiO_2)_x$ alloys

Vickers hardness of $Sn_{80-x}Al_{20}(TiO_2)_x$ alloys at 10 gram force and indentation time 5 sec are shown in Table 7. The minimum shear stress (τ_m) value of $Sn_{80-x}Al_{20}(TiO_2)_x$ alloys was calculated then listed in Table 7. Little variation occurred in Vickers hardness of $Sn_{80}Al_{20}$ alloy after adding TiO_2 nanoparticles.

Table 7:- Vickers hardness and minimum shear stress of $Sn_{80-x}Al_{20}(TiO_2)_x$ alloys

Alloys	H_v kg/mm^2	μ_n kg/mm^2
$Sn_{80}Al_{20}$	36.43±2.7	14.33
$Sn_{79.5}Al_{20}(TiO_2)_{0.5}$	35.77±1.9	11.80
$Sn_{79}Al_{20}(TiO_2)_1$	37.88±2.2	12.50
$Sn_{78.5}Al_{20}(TiO_2)_{.1.5}$	38.92±3.1	12.84

Effect of adding TiO_2 on thermal properties and electrical resistivity of Sn-Al alloy

Figure 8 shows DSC thermographs for $Sn_{80-x}Al_{20}(TiO_2)_x$ alloys. Little variation occurred in exothermal peak of $Sn_{80}Al_{20}$ alloy. The melting temperature and other thermal properties of $Sn_{80-x}Al_{20}(TiO_2)_x$ alloys are listed in Table 8. Melting temperature of $Sn_{80}Al_{20}$ alloy increased after adding TiO_2 nanoparticles.

Electrical resistivity and calculated thermal conductivities of $Sn_{80-x}Al_{20}(TiO_2)_x$ alloys are listed in Table 8. Electrical resistivity of $Sn_{80}Al_{20}$ alloy varied after adding TiO_2 nanoparticles. That is because TiO_2 nanoparticles dissolved in the Sn matrix playing as scattering center for conduction electrons caused a change in Sn matrix.

Table 8:- electric resistivity and other thermal properties of $Sn_{80-x}Al_{20}(TiO_2)_x$ alloys

Alloys	ρ x10^{-6} Ω.cm	K W $m^{-1}K^{-1}$	C_p x 10^3 J/g. ºC	ΔS J/g. ºC	Melting point ºC
$Sn_{80}Al_{20}$	67.3	1.21	0.723	0.122	227.03

$Sn_{79.5}Al_{20}(TiO_2)_{0.5}$	137.30	2.1	3.74	0.198	228.22
$Sn_{79}Al_{20}(TiO_2)_1$	77.76	2.31	2.85	0.190	228.92
$Sn_{78.5}Al_{20}(TiO_2)_{1.5}$	68.40	3.27	3.34	0.2	229.63

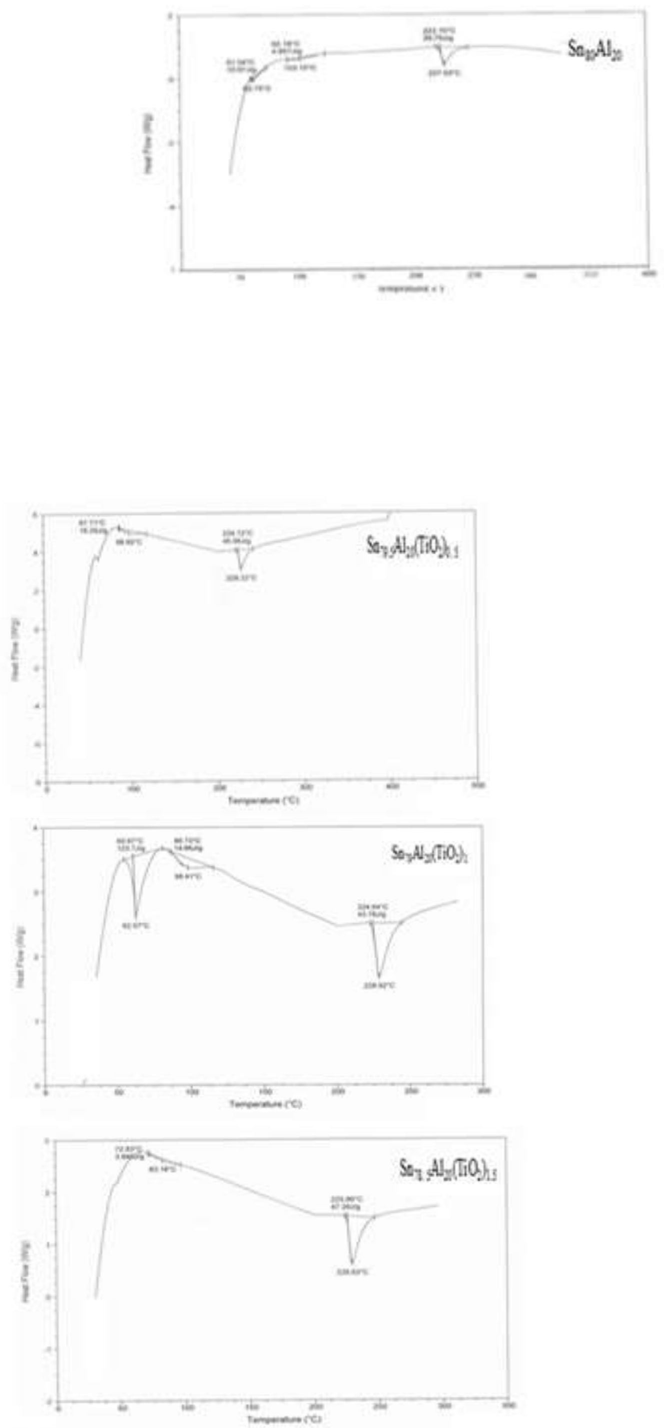

Figure 8:- DSC of $Sn_{80-x}Al_{20}(TiO_2)_x$ alloys

Conclusion

Structure of $Sn_{87}Sb_{10}Pb_3$ and $Sn_{80}Al_{20}$ alloys changed after adding TiO_2 nanoparticles. Elastic modulus and Vickers hardness of $Sn_{87}Sb_{10}Pb_3$ and $Sn_{80}Al_{20}$ alloys increased after adding TiO_2 nanoparticles. Internal friction and mmelting temperature of $Sn_{87}Sb_{10}Pb_3$ alloy decreased but internal friction and melting temperature of $Sn_{80}Al_{20}$ alloy increased after adding TiO_2 nanoparticles. The $Sn_{85.5}Sb_{10}Pb_3(Ti_2O)_{1.5}$ alloy has beast properties for automotive industry. Also $Sn_{78.5}Al_{20}(Ti_2O)_{1.5}$ alloy has beast properties for marine applications.

References

[1] Forrester P. G, Met. Rev. 5 **(**1960**)** 507
[2] Pratt G. C, Int. Met. Rev. 18 (1973) 62
[3] Forrester P. G, Curr. Engg. Pract 3 (1961) 4
[4] Tegart W. I. M, Elements of mechanical metallurgy (New York: The MacMillan Co.) (1966) 91
[5] Desaki T, Goto Y, Kamiya S, JSAE Rev. 21 (2000) 321
[6] Lepper K, James M, Chashechkina J, Rigney D. A, Wear 46 (1997) 203
[7] Perrin C, S. Harris, McCartney D. G, Syngellakis S, Reed P. A, in: J.F. Morton, B.C. Muddle (Eds.), Mater. Forum 28 (2004) 1371
[8] Kong C. J, Brown P. D, S, Harris J, McCartney D. G, Mater. Sci. Eng. A 403 (2005) 205
[9] Ning X. J, Jang J. H, Kim H. J, Li C. J, C. Lee, Surf. Coat. Technol. 202 (2008) 1681
[10] Ning X. J, Kim J. H, Kim H. J, Lee C, Applied Surface Science 255 (2009) 3933
[11] Pathak J. P and Mohan S, Bull. Mater. Sci. 26:3 (2003) 315
[12] Kama M, El-Bediwi A and El-Shobaki M, Radia. Eff. Def. Sol. 161 (2006) 549
[13] Bora M. O, Coban O, Sinmazcelik T, Gunay V, Zeren M, Mater. Design 31 (2010) 2707
[14] El- Bediwi A. B, El Said Gouda, Kamal M, AMSE, 65, n° 1, Modeling C- 2004
[15] Kamal M, Abdel-Salam A, Pieri J. C, J. Mater. Sci. 19 (1984) 3880
[16] El-Bediwi A, Lashin A, Mossa M, Kamal M, Mater. Sci. Eng. A 528 (2011) 3568
[17] E Schreiber, Anderson O. L and Soga N, Elastic constant and their measurements, McGraw-Hill, New York, (1973) 82
[18] Timoshenko S and Goddier J. N, "Theory of elasticity, 2nd Ed", McGraw-Hill, New York, (1951) 277
[19] Nuttall K, J. Inst. Met. 99 (1971) 266